

# Weinberg Eigenvalues and Pairing with Low-Momentum Potentials

S. Ramanan <sup>a,b</sup>, S.K. Bogner <sup>a,c</sup>, and R.J. Furnstahl <sup>a</sup>

<sup>a</sup>*Department of Physics, The Ohio State University, Columbus, OH 43210*

<sup>b</sup>*Center for High Energy Physics, Indian Institute of Science, Bangalore 560012*

<sup>c</sup>*National Superconducting Cyclotron Laboratory and Department of Physics and Astronomy, Michigan State University, East Lansing, MI 48844*

---

## Abstract

The nonperturbative nature of nucleon-nucleon interactions evolved to low momentum has recently been investigated in free space and at finite density using Weinberg eigenvalues as a diagnostic. This analysis is extended here to the in-medium eigenvalues near the Fermi surface to study pairing. For a fixed value of density and cutoff, the eigenvalues increase arbitrarily in magnitude close to the Fermi surface, signaling the pairing instability. When using normal-phase propagators, the Weinberg analysis with complex energies becomes a form of stability analysis and the pairing gap can be estimated from the largest attractive eigenvalue. With Nambu-Gorkov Green's functions, the largest attractive eigenvalue goes to unity close to the Fermi surface, indicating the presence of bound states (Cooper pairs), and the corresponding eigenvector leads to the self-consistent gap function.

---

## 1 Introduction

The perturbativeness of a nucleon-nucleon (NN) potential can be quantified using the eigenvalue analysis introduced long ago by Weinberg [1]. Consider the operator Born series for the free-space  $T$ -matrix at energy  $E$ :

$$T(E) = V + V \frac{1}{E - H_0} V + \dots \quad (1)$$

---

*Email addresses:* suna@pacific.ohio-state.edu (S. Ramanan), bogner@mps.ohio-state.edu (S.K. Bogner), furnstahl.1@osu.edu (R.J. Furnstahl).

By finding the eigenvalues and eigenvectors of

$$\frac{1}{E - H_0} V |\Psi_\nu\rangle = \eta_\nu(E) |\Psi_\nu\rangle, \quad (2)$$

and then acting with  $T(E)$  on the eigenvectors,

$$T(E) |\Psi_\nu\rangle = V |\Psi_\nu\rangle (1 + \eta_\nu + \eta_\nu^2 + \dots), \quad (3)$$

it follows that nonperturbative behavior at energy  $E$  is signaled by one or more eigenvalues with  $|\eta_\nu(E)| \geq 1$  [1,2]. Such an analysis has been recently used as a diagnostic of low-momentum potentials in free space [3,4,5]. Major decreases in the magnitudes of the largest eigenvalues were observed as bare nucleon-nucleon potentials (such as those from Refs. [6,7]) were evolved using renormalization group (RG) methods [8,9]. These decreases can be linked to a dampening of the sources of nonperturbative physics, such as the repulsive core and the short-range tensor interaction, as the cutoff is lowered. Lowering  $\Lambda$  yields a soft potential (generically called “ $V_{\text{low } k}$ ”), which in turn simplifies few and many-body calculations [10,11].<sup>1</sup>

The Weinberg analysis was extended to the in-medium T-matrix in Ref. [10] to examine the effect of Pauli blocking. The conclusion was that the bulk nuclear matter energy calculations are perturbative in the particle-particle channel. The focus in Ref. [10] was primarily on repulsive eigenvalues, which are tied to short-range physics. But questions naturally arise about other sources of non-perturbative physics. In this paper we extend the in-medium eigenvalue analysis to energies close to the Fermi surface, where the attractive NN interaction leads to a pairing instability in the particle-particle channel. This nonperturbative feature should be reflected in the Weinberg eigenvalues. Verifying the eigenvalue analysis for pairing is also a step toward a more general application of this tool to long-range correlations in the particle-hole channel.

In Sec. 2, we review the in-medium results and focus on the Weinberg eigenvalues for energies close to the Fermi surface. This takes the form of a stability analysis with complex energies [13]. From the eigenvalues it is possible to estimate the BCS gaps. Pairing is naturally taken into account in the Nambu-Gorkov formalism. Using the two-particle Nambu-Gorkov Green’s function we evaluate the Weinberg eigenvalues in Sec. 3, first for a separable model

---

<sup>1</sup> There are various RG methods used to generate low-momentum potentials, including using sharp and smooth regulators and through the Similarity Renormalization Group (SRG) [5]. SRG potentials depend on a parameter  $\lambda$ , which measures the spread of the off-diagonal strength and acts as a cutoff. We restrict our calculations here to sharp-cutoff  $V_{\text{low } k}$  potentials; gaps with smooth regulators are discussed in Ref. [12].

and then for a  $V_{\text{low } k}$  potential. Throughout this paper we work at zero temperature, with only a two-body potential and a free single-particle spectrum. Moreover we consider only the  $^1S_0$  partial wave, although the analysis can be applied more generally and the cutoff dependence of the extracted gap used to test the importance of three-body forces in other partial-wave channels. We summarize our findings and discuss future investigations in Sec. 4.

## 2 In-medium Weinberg Eigenvalues and the Pairing Gap

In free space, the Weinberg eigenvalue analysis refers to the spectrum of  $VG_{pp}^0$  as in Eq. (2), where  $G_{pp}^0$  is the two-body non-interacting particle-particle Green's function:

$$G_{pp}^0(E) = \frac{1}{E - H_0} . \quad (4)$$

As noted above, when the magnitude of the largest eigenvalue lies outside the unit circle, i.e.,  $|\eta_\nu(E)| \geq 1$ , the corresponding Born series expansion for the  $T$  matrix no longer converges. Lowering the cutoff results in a softening of the short-range repulsion and the iterated tensor force in free space, while the impact of shallow bound states in the S waves is eliminated at sufficiently high density due to Pauli-blocking. As a result the eigenvalues decrease in magnitude as the cutoff is lowered. In free space, for any value of the cutoff there are only a finite number of eigenvalues which lie outside the unit circle [1].

The same conclusions hold in-medium as long as we work at energies away from the Fermi-surface [3,10]. Figure 1 shows the largest attractive and repulsive eigenvalues at center of mass energy  $E = 0$  MeV for neutron matter in the  $^1S_0$  channel for three different values of the cutoff  $\Lambda$ .<sup>2</sup> We note that lowering the cutoff and increasing the density both contribute to dampening the sources of nonperturbative physics, which is reflected by the smaller magnitudes of the eigenvalues at finite densities, consistent with the nuclear matter results of Ref. [10].

Close to the Fermi surface, the attractive interaction between the particles leads to the normal ground state becoming unstable to the formation of Cooper pairs. While considering the behavior of the eigenvalues away from the Fermi surface (e.g., for analyzing bulk properties), it is sufficient to consider only

---

<sup>2</sup> At negative energy, the purely real free-space Weinberg eigenvalues can be viewed as inverse coupling constants that the interaction must be scaled by to support a bound state at that energy. Therefore, negative and positive Weinberg eigenvalues are called repulsive and attractive eigenvalues. The same designations are used for positive-energy eigenvalues, which are complex, according to whether they are continuations from repulsive or attractive eigenvalues at negative energy.

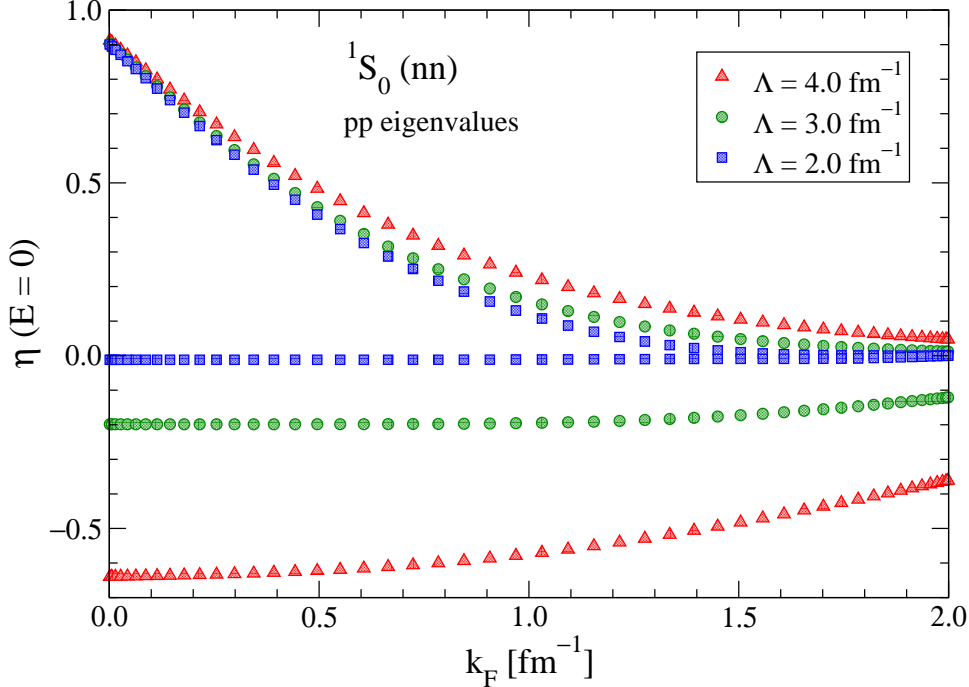


Fig. 1. Largest attractive ( $\eta > 0$ ) and repulsive ( $\eta < 0$ ) eigenvalues at  $E = 0$  MeV for neutron matter in the  $^1S_0$  channel for three different cutoffs, as a function of Fermi momentum  $k_F$ .

the particle-particle Green's function, because the phase space for hole propagation is small [14]. Investigating the signatures of pairing, however, requires us to consider the hole propagation as well, since the phase space around the Fermi surface becomes important.

The in-medium Weinberg eigenvalue equation including the hole propagation is:

$$G_{pphh}^0(E)V|\Psi_\nu(E)\rangle = \eta_\nu(E)|\Psi_\nu(E)\rangle, \quad (5)$$

where  $G_{pphh}^0(E)$  is the in-medium two-particle and two-hole non-interacting propagator. In momentum space, this propagator is given by [14]:

$$G_{pphh}^0(\vec{k}_1, \vec{k}_2; \omega) = \frac{\theta(|\vec{k}_1| - k_F)\theta(|\vec{k}_2| - k_F)}{\omega - \varepsilon(\vec{k}_1) - \varepsilon(\vec{k}_2) + i\epsilon} - \frac{\theta(k_F - |\vec{k}_1|)\theta(k_F - |\vec{k}_2|)}{\omega - \varepsilon(\vec{k}_1) - \varepsilon(\vec{k}_2) - i\epsilon}, \quad (6)$$

where  $\vec{k}_1$  and  $\vec{k}_2$  are the momenta of the particles (holes),  $k_F$  is the Fermi momentum, and  $\omega$  is the two-particle excitation energy measured from the Fermi surface. The above propagator represents propagation of two particles above the Fermi surface and two holes below the Fermi surface. We use the free-particle spectrum to be consistent with the usual BCS treatment applied in Refs. [12], [15], and [16].

The phase space for pairing is maximal for back-to-back pairs [13], therefore

we apply Eq. (6) with zero center-of-mass momentum,

$$G_{pphh}^0(k, \omega) = \frac{\theta(k - k_F)}{\omega - 2\varepsilon(k) + i\epsilon} - \frac{\theta(k_F - k)}{\omega - 2\varepsilon(k) - i\epsilon}, \quad (7)$$

where  $\vec{k}$  is the relative momentum. With  $\omega = E - 2\mu$  and  $\varepsilon(k) = k^2/2 - \mu$ , where  $\mu = k_F^2/2$  is the zero-temperature, non-interacting Fermi energy (we use units in which  $\hbar^2/m_N = 1$ , with  $m_N$  the mass of a nucleon), the in-medium propagator is simply

$$G_{pphh}^0(k, E = k_0^2) = \frac{\theta(k - k_F)}{k_0^2 - k^2 + i\epsilon} - \frac{\theta(k_F - k)}{k_0^2 - k^2 - i\epsilon}. \quad (8)$$

We now study the Weinberg eigenvalues for the kernel  $G_{pphh}^0(E)V_{\text{low } k}$ . Just as for the free-space case [3], we actually solve for the eigenvalues of  $V_{\text{low } k}G_{pphh}^0(E)$ , which has the same eigenvalue spectrum but allows for direct integration over singularities. In a given partial wave, the Weinberg eigenvalue equation is:

$$\frac{2}{\pi} \int_0^\Lambda q^2 dq V_{\text{low } k}(k, q) \left( \frac{\theta(q - k_F)}{k_0^2 - q^2 + i\epsilon} - \frac{\theta(k_F - q)}{k_0^2 - q^2 - i\epsilon} \right) \Psi_\nu(q) = \eta_\nu(k_0^2) \Psi_\nu(k). \quad (9)$$

For notational convenience we have suppressed the energy dependence of the eigenvectors in Eq. (9). Using the standard identities,

$$\frac{1}{x - x_0 \pm i\epsilon} = \mathcal{P} \frac{1}{x - x_0} \mp i\pi \delta(x - x_0), \quad (10)$$

$$\delta(f(x)) = \sum_i \frac{\delta(x - x_i)}{|f'(x)|_{x=x_i}}, \quad (11)$$

Eq. (9) becomes:

$$\begin{aligned} \frac{2}{\pi} \mathcal{P} \int_0^\Lambda q^2 dq V_{\text{low } k}(k, q) \left( \frac{\theta(q - k_F) - \theta(k_F - q)}{k_0^2 - q^2} \right) \Psi_\nu(q) \\ - ik_0 V_{\text{low } k}(k, k_0) \Psi_\nu(k_0) = \eta_\nu(k_0^2) \Psi_\nu(k). \end{aligned} \quad (12)$$

To identify signatures of pairing, we plot in Fig. 2 the magnitude of the largest attractive and repulsive Weinberg eigenvalues for  $G_{pphh}^0 V$  as a function of density for the  $^1S_0$  partial wave with center-of-mass energy  $E = 50$  MeV. The  $V_{\text{low } k}$  matrix elements are from the Argonne  $v_{18}$  potential [6] using a sharp regulator, but the results here apply generally to all low-momentum potentials. As we scan through  $k_F$ , the largest repulsive eigenvalue for larger cutoffs shows a cusp behavior due to the sharp Fermi surface that is localized near the momentum corresponding to  $k_F = \sqrt{E}$ . The repulsive eigenvalues are strongly cutoff dependent and no cusp is resolved at the lower cutoffs. In

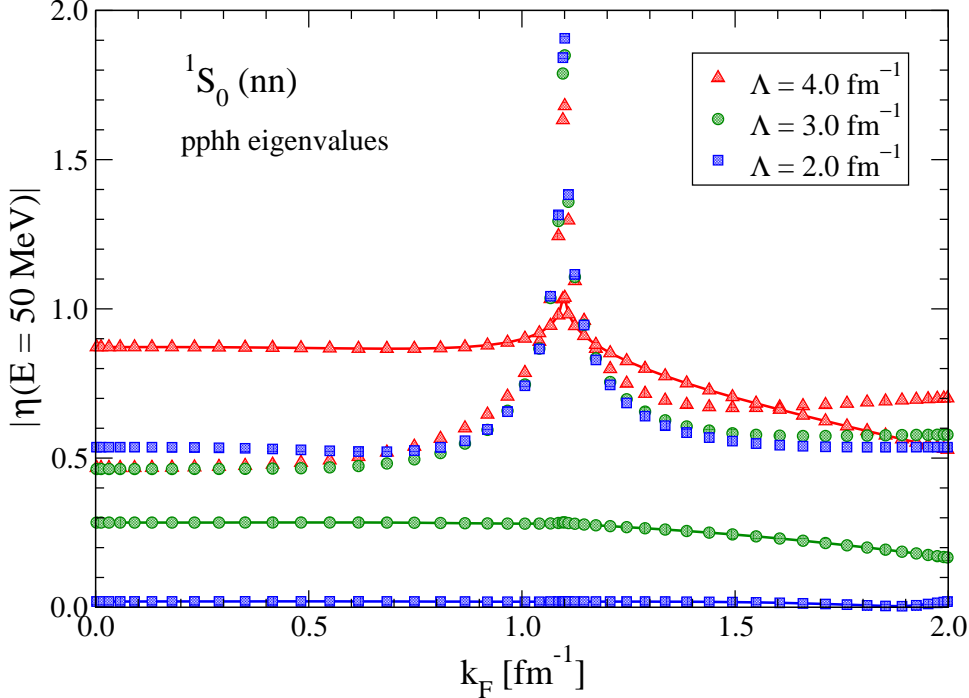


Fig. 2. Magnitudes of the largest attractive and repulsive eigenvalues at  $E = 50$  MeV as a function of Fermi momentum  $k_F$  for neutron matter in the  $^1S_0$  channel for three different cutoffs using the two-particle and two-hole propagator. (The repulsive eigenvalues are connected by lines.)

contrast, the attractive eigenvalues depend weakly on cutoff and show a broad cusp near the Fermi surface; this behavior is the link to the pairing instability. Similarly, Fig. 3 shows the largest attractive eigenvalue at a fixed density (in this case  $k_F = 1.0 \text{ fm}^{-1}$ ) as a function of  $E$  at several cutoffs. Again we find weak cutoff dependence and a broad cusp about the Fermi surface; in the next section we extract the gap from this behavior by going to complex energies.

### 2.1 Stability Analysis and Pairing gaps

In this section we adapt the stability analysis of Ref. [13]. Consider Eq. (8) for the two-particle and two-hole non-interacting Green's function. Above  $2\mu$  we have the particle-particle continuum and below  $2\mu$  we have the hole-hole continuum. Therefore, a stable bound state around  $2\mu$  cannot be accommodated. In fact, the bound-state energies measured from the Fermi surface  $2\mu$  are purely imaginary and have a value of  $\pm i\Delta_F$ , where  $\Delta_F$  is the BCS gap at  $k_F$  [13,17] (actually just an approximation, see below). This result can be easily established by studying the singularity structure of the in-medium  $T$  matrix in the complex plane [13]. Two purely imaginary poles of the  $T$  matrix appear for an attractive two-body interaction between the pairs and the normal phase becomes unstable. Therefore, at  $E = 2\mu \pm i\Delta_F$  the magnitude of the largest

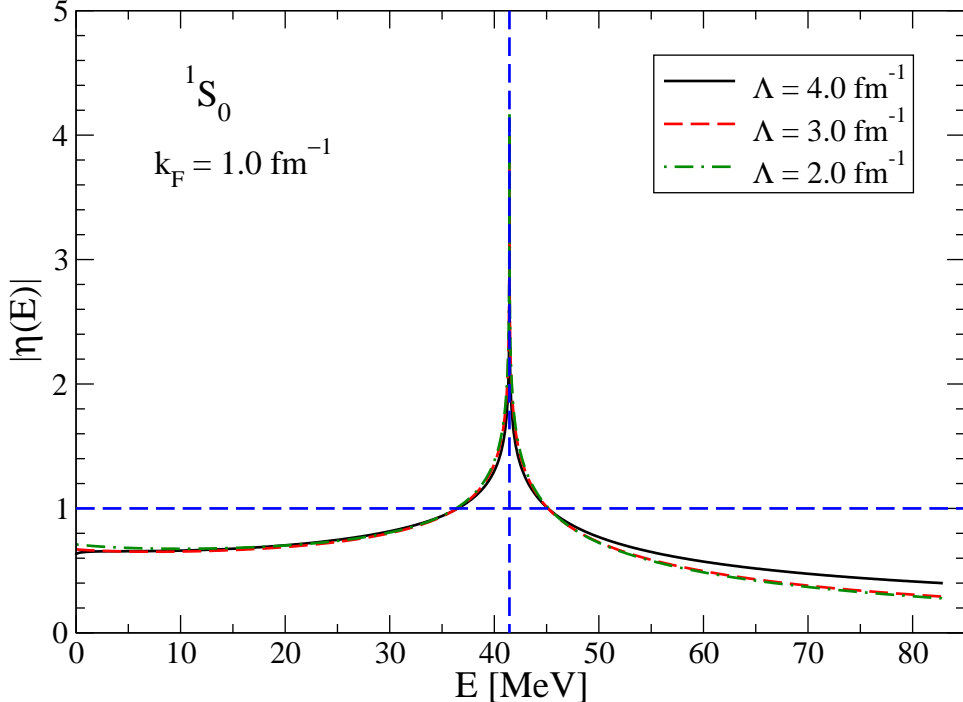


Fig. 3. Magnitude of the largest attractive eigenvalue for neutron matter as a function of energy  $E$  in the  $^1S_0$  channel for three different cutoffs using the two-particle and two-hole propagator.

attractive eigenvalue  $|\eta(2\mu \pm i\Delta_F)|$  equals one, signaling the presence of a bound state at these energies. Dialing the imaginary part of  $2\mu \pm iE_0$  from negative energies through 0 to positive energies leads to eigenvalues that start to grow as  $E_0$  increases, cross one at  $E_0 = \pm\Delta_F$  and become singular as  $E_0 \rightarrow 0$ . The eigenvalues are symmetric about  $E_0 = 0$ .

This behavior is seen in Fig. 4, where we plot the largest attractive Weinberg eigenvalue in the  $^1S_0$  channel for neutron matter at  $k_F = 1.0 \text{ fm}^{-1}$  for a cutoff of  $\Lambda = 2.0 \text{ fm}^{-1}$ . The value of the imaginary part of the energy where the eigenvalue crosses one ( $E_c$ ) directly gives a first approximation to the pairing gap. In Fig. 5 we show the corresponding density dependence of the pairing gaps extracted via the stability analysis for several cutoffs compared to self-consistent gaps obtained from the BCS gap equation [12]. Note that we are working in the limit where  $\Delta_F/\mu$  is small, so that the gap is independent of the momentum  $k$  and depends only on the density  $k_F$ . The errors in the gaps obtained from the stability analysis scale as a power of  $\Delta_F/\mu$ . Thus the in-medium Weinberg eigenvalues not only reflect the instability of the normal phase, they also give a good estimate of the pairing gap. For the range of cutoffs ( $\Lambda = 1.6 \text{ fm}^{-1}$  to  $2.5 \text{ fm}^{-1}$ ) considered here, Fig. 5 shows that the gaps exhibit very weak cutoff dependence, as was found in Ref. [12].

The gap can be cleanly extracted from the stability analysis at lower cutoffs because the effect of other sources of non-perturbative physics has been damp-

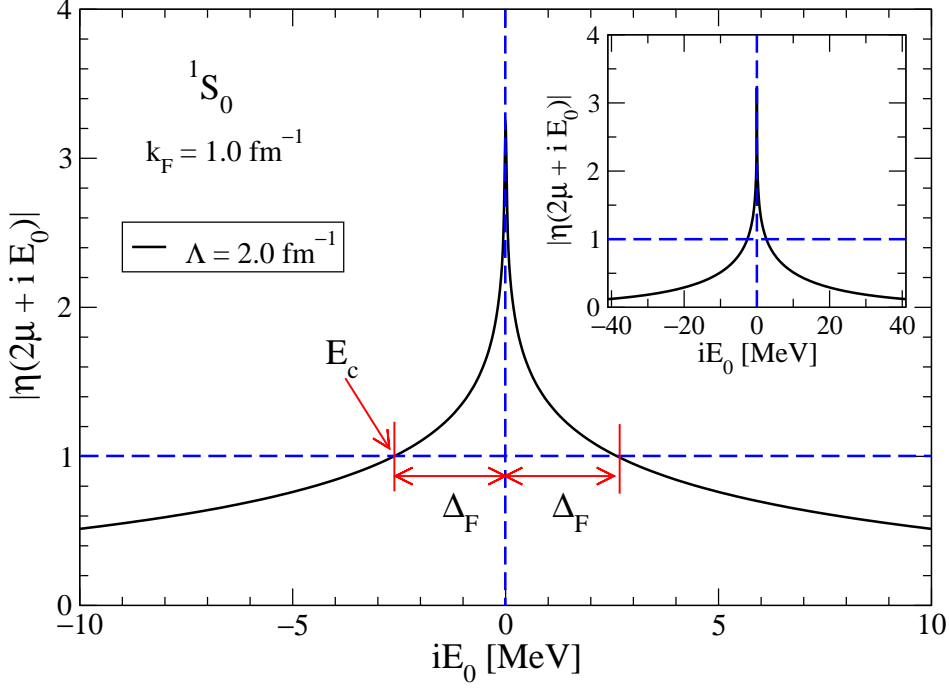


Fig. 4. Largest attractive eigenvalue as a function of energy  $iE_0$  (scanning along the imaginary axis).  $E_c$  refers to the critical energy for which  $|\eta_\nu| = 1$ ; in this case  $E_c \approx \Delta_F$ , the BCS gap at  $k_F$ .

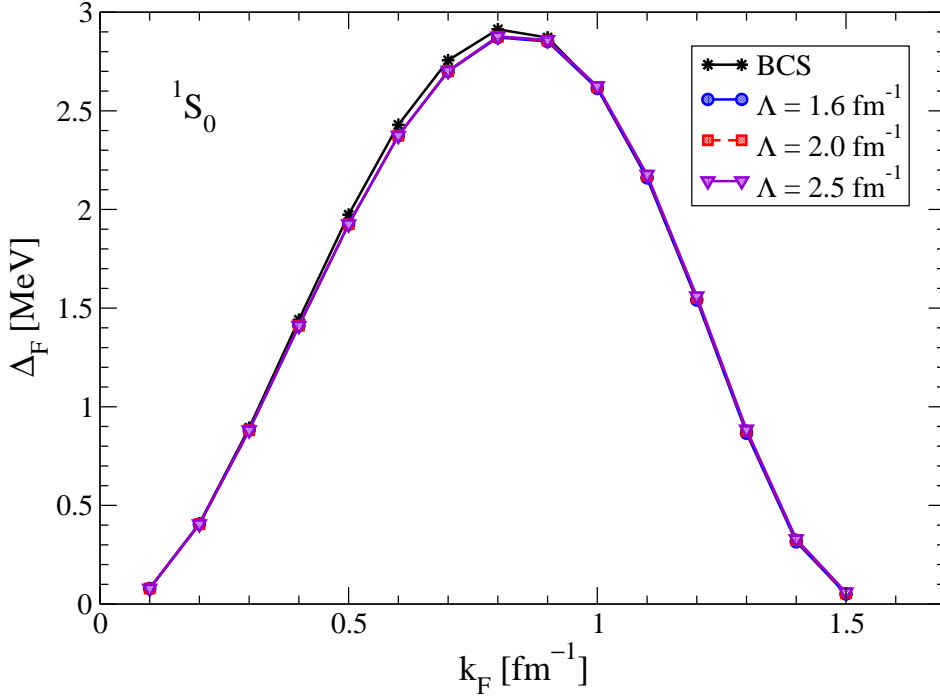


Fig. 5. Density dependence of the gap extracted through the stability analysis for neutron matter at several different cutoffs  $\Lambda$  compared to the self-consistent gaps obtained from the BCS gap equation.

ened, leaving the largest attractive eigenvalue isolated. The analysis is more involved at higher cutoffs, but still possible in the  $^1S_0$  channel, where repulsive eigenvalues corresponding to the strong short-range repulsion dominate. By continuing the attractive eigenvalue from zero energy, where it is cleanly distinguished, to the Fermi surface, gaps can be extracted at all cutoffs. As in Fig. 5, these agree well with the BCS gaps and show only very small cutoff dependence at all higher cutoffs.

### 3 Weinberg Eigenvalues in the Nambu-Gorkov Formalism

Thus far we have worked in the normal phase with the non-interacting propagator. Here we consider the Weinberg eigenvalue analysis in the paired phase using the Nambu-Gorkov formalism. In momentum space for a homogeneous system, the corresponding Nambu-Gorkov Green's function reduces to [18]

$$G_{\text{NG}}^0(\vec{k}, \omega) = \int \frac{d\omega'}{2\pi i} \left[ \mathcal{G}(\vec{k}, (\omega)) \tilde{\mathcal{G}}(\vec{k}, \omega - \omega') + \mathcal{F}(\vec{k}, \omega) \mathcal{F}^\dagger(\vec{k}, \omega - \omega') \right], \quad (13)$$

where the normal and anomalous propagators are given by

$$\mathcal{G}(\vec{k}, \omega) = \frac{u_k^2}{\omega - E_k + i\epsilon} + \frac{v_k^2}{\omega + E_k - i\epsilon}, \quad (14)$$

$$\tilde{\mathcal{G}}(\vec{k}, \omega) = -\frac{u_k^2}{\omega + E_k - i\epsilon} - \frac{v_k^2}{\omega - E_k + i\epsilon}, \quad (15)$$

$$\mathcal{F}(\vec{k}, \omega) = \mathcal{F}^\dagger(\vec{k}, \omega) = -u_k v_k \left( \frac{1}{\omega - E_k + i\epsilon} - \frac{1}{\omega + E_k - i\epsilon} \right). \quad (16)$$

The spectral functions  $u_k$  and  $v_k$  are defined as

$$u_k^2 = \frac{1}{2} \left( 1 + \frac{\xi_k}{E_k} \right), \quad v_k^2 = \frac{1}{2} \left( 1 - \frac{\xi_k}{E_k} \right), \quad (17)$$

with

$$E_k = \sqrt{\xi_k^2 + \Delta(k)^2}. \quad (18)$$

Here  $\xi_k = \varepsilon_k - \mu$  is the single-particle energy measured from the chemical potential  $\mu$ , which for a non-interacting system at zero temperature is  $\mu = k_F^2/2$ . In Eq. (18),  $\Delta(k)$  is the gap function. Evaluating the contour integral in Eq. (13) we get the following expression for the two-particle Nambu-Gorkov propagator,

$$G_{\text{NG}}^0(\vec{k}, \omega) = \frac{u_k^2}{\omega - 2E_k + i\epsilon} - \frac{v_k^2}{\omega + 2E_k - i\epsilon}. \quad (19)$$

Taking the  $\Delta(k) \rightarrow 0$  limit reproduces the non-interacting two-particle  $G_{pphh}^0$  propagator.

The Weinberg eigenvalue equation is (with  $E = \omega + 2\mu$ )

$$G_{\text{NG}}^0(k, E)V|\Psi_\nu(E)\rangle = \eta_\nu^{\text{NG}}(E)|\Psi_\nu(E)\rangle . \quad (20)$$

At  $E = 2\mu$  the eigenvalue problem can be reduced to the BCS gap equation. To see this, we start with Eq. (20) for a general potential in momentum space,

$$\frac{2}{\pi} \int_0^\Lambda k^2 dk G_{\text{NG}}^0(k', E)V(k', k)\Psi_\nu(k, E) = \eta_\nu^{\text{NG}}(E)\Psi_\nu(k', E) . \quad (21)$$

As noted earlier, we can solve the above equation by converting it to a left-eigenvalue problem, or alternatively solve the right-eigenvalue problem,

$$VG_{\text{NG}}^0(z)[V|\Psi_\nu(z)\rangle] = \eta_\nu^{\text{NG}}(z)[V|\Psi_\nu(z)\rangle] , \quad (22)$$

which has the same spectrum as  $G_{\text{NG}}^0(z)V$ , and integrate over the singularity directly. Using the two-particle Nambu-Gorkov propagator, Eq. (22) can be written as

$$\begin{aligned} \frac{2}{\pi} \int_0^\Lambda k^2 dk V(k', k) \left( \frac{u_k^2}{\omega - 2E_k + i\epsilon} - \frac{v_k^2}{\omega + 2E_k - i\epsilon} \right) \Psi_\nu(k, E) \\ = \eta_\nu^{\text{NG}}(E)\Psi_\nu(k', E) . \end{aligned} \quad (23)$$

For  $\omega = 0$  (i.e.,  $E = 2\mu$ ) and with  $E_k = \sqrt{\xi_k^2 + \Delta(k)^2}$ , Eq. (23) has a solution with  $\eta_\nu^{\text{NG}}(2\mu) = 1$ :

$$-\frac{1}{\pi} \int_0^\Lambda k^2 dk V(k', k) \left( \frac{1}{\sqrt{\xi_k^2 + \Delta(k)^2}} \right) \Psi_\nu(k, 2\mu) = \Psi_\nu(k', 2\mu) , \quad (24)$$

which is equivalent to the gap equation with the corresponding eigenvector  $\Psi_\nu(k, E \rightarrow 2\mu)$  equal to the gap function  $\Delta(k)$ . However, it is not clear how to derive  $\Delta(k)$  from the eigenvalue equation because of the dependence of  $E_k$  on  $\Delta(k)$ ; simple iterations do not lead to self-consistency. At energies of  $2\mu \pm 2\Delta_F$ , the eigenvalue in Eq. (23) becomes singular, see Fig. 6. This coincides with the branch point of the two-particle Green's function and can be associated with the breaking of the pairs.

To illustrate the behavior near the Fermi surface, we first calculate the Weinberg eigenvalues of the Nambu-Gorkov propagator using a separable potential of the form

$$V = \lambda|f\rangle\langle f| , \quad (25)$$

where  $\lambda$  is a coupling that controls the strength of the potential.  $\lambda$  is negative for an attractive potential and positive for a repulsive potential. The Weinberg eigenvalue equation in momentum space is

$$\frac{2}{\pi} \lambda \langle f|\Psi_\nu(E)\rangle \int_0^\Lambda k^2 dk G_{\text{NG}}^0(k, E)\langle k|f\rangle|k\rangle = \eta_\nu^{\text{NG}}(E)|\Psi_\nu(E)\rangle . \quad (26)$$

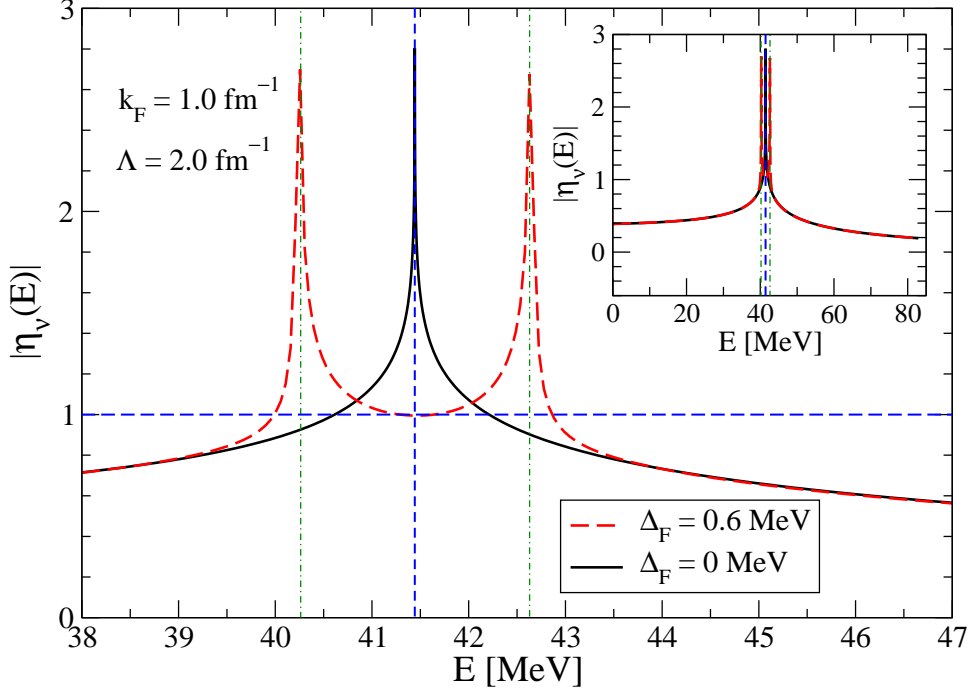


Fig. 6. Plot of the Weinberg eigenvalue for the separable potential of Eqs. (25) and (30) as a function of  $E$  for both  $\Delta_F = 0$  MeV and  $\Delta_F \approx 0.604$  MeV. The solid line represents the eigenvalue for the non-interacting propagator,  $G_{pphh}^0$ , while the dashed lines is for the Nambu-Gorkov propagator,  $G_{\text{NG}}^0$ . The Nambu-Gorkov eigenvalue  $\eta_\nu^{\text{NG}}$  goes to one close to  $2\mu$ , indicating formation of a Cooper pair. Large singular values for  $\eta_\nu^{\text{NG}}$  are observed at  $2\mu \pm 2\Delta_F$ , which represents the energy at which the pairs are broken.

From Eq. (26), we see that there is only one Weinberg eigenvalue for any rank-one separable potential, which is given by

$$\eta_\nu^{\text{NG}}(E) = \lambda \langle f | \Psi_\nu(E) \rangle, \quad (27)$$

and the corresponding eigenvector is

$$|\Psi_\nu(E)\rangle = \frac{2}{\pi} \int_0^\Lambda k^2 dk G_{\text{NG}}^0(k, E) f(k) |k\rangle. \quad (28)$$

Substituting Eq. (28) into Eq. (27), we get the following closed expression for the Weinberg eigenvalue:

$$\eta_\nu^{\text{NG}}(E) = \lambda \frac{2}{\pi} \int_0^\Lambda k^2 dk G_{\text{NG}}^0(k, E) |f(k)|^2. \quad (29)$$

For simplicity we choose the function  $f(k)$  to be a gaussian,

$$f(k) = e^{-k^2/\alpha^2}, \quad (30)$$

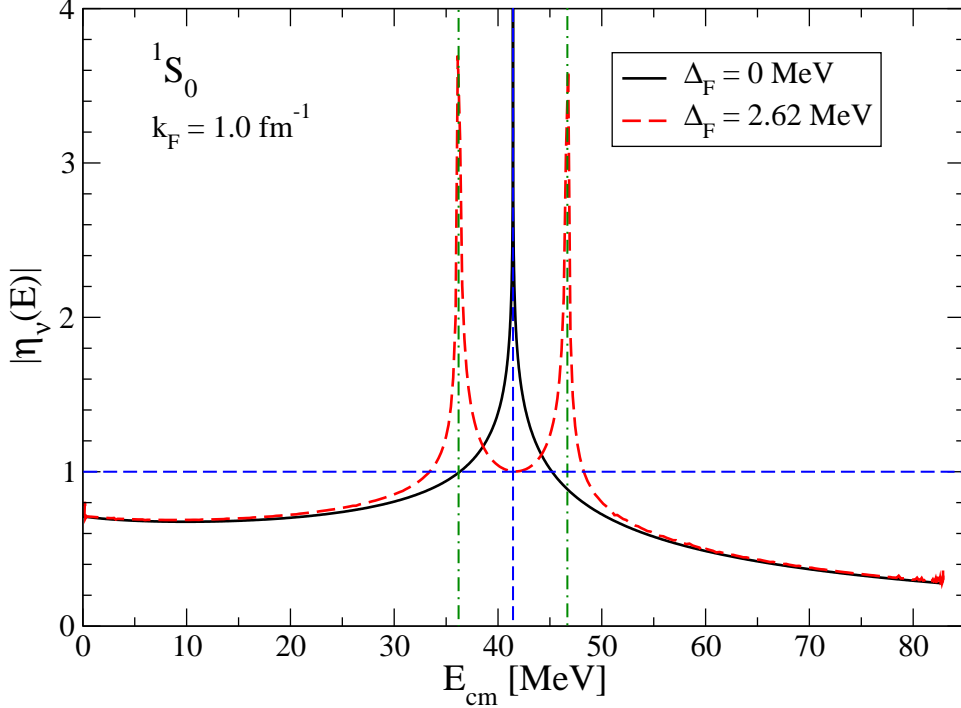


Fig. 7. Largest attractive Weinberg eigenvalue as a function of energy  $E$  for a cutoff  $\Lambda = 2.0 \text{ fm}^{-1}$  at  $k_F = 1.0 \text{ fm}^{-1}$ . Notice that as  $E \rightarrow 2\mu$ ,  $\eta_\nu(E)$  tend to one.

with  $\alpha = \sqrt{2} \text{ fm}^{-1}$ . We also set  $\lambda = -1 \text{ fm}$ , so that the separable potential is attractive. Figure 6 shows the Weinberg eigenvalue for the separable gaussian potential as a function of center-of-mass energy  $E$  for  $\Delta_F = 0 \text{ MeV}$  and for finite  $\Delta_F$ .

For vanishing  $\Delta_F$ , the eigenvalue becomes singular at  $E = 2\mu$  due to the sharp Fermi surface. For the gapped phase, the gap function appearing in the NG propagators can be estimated from the normal-phase Weinberg analysis for which  $\eta_\nu(2\mu + i\Delta_F) = 1$ . In the present separable example, the normal-phase estimate gives  $\Delta_F \approx 0.604 \text{ MeV}$ . This value is taken as the initial guess for the gap function,  $\Delta(k) \approx \Delta_F$ , which is then used in the two-particle Nambu-Gorkov propagator and the corresponding eigenvalue is evaluated using

$$\eta_\nu^{\text{NG}}(E) = \lambda \frac{2}{\pi} \int_0^\Lambda k^2 dk |f(k)|^2 \left( \frac{u_k^2}{\omega - 2E_k + i\epsilon} - \frac{v_k^2}{\omega + 2E_k - i\epsilon} \right), \quad (31)$$

where  $\omega = E - 2\mu$ , and  $E_k = \sqrt{\xi_k^2 + \Delta_F^2}$ . We see that the eigenvalue  $\eta_\nu^{\text{NG}}(E)$  tends to one close to  $E = 2\mu$ , as expected.

Figure 7 shows the largest attractive Weinberg eigenvalue as a function of  $E$  for  $V_{\text{low } k}$  in the  $^1S_0$  partial wave at  $k_F = 1.0 \text{ fm}^{-1}$  for a cutoff  $\Lambda = 2.0 \text{ fm}^{-1}$ . As with the separable example, the gap function  $\Delta(k)$  appearing in the NG propagators is taken from the normal-phase Weinberg eigenvalue estimate.

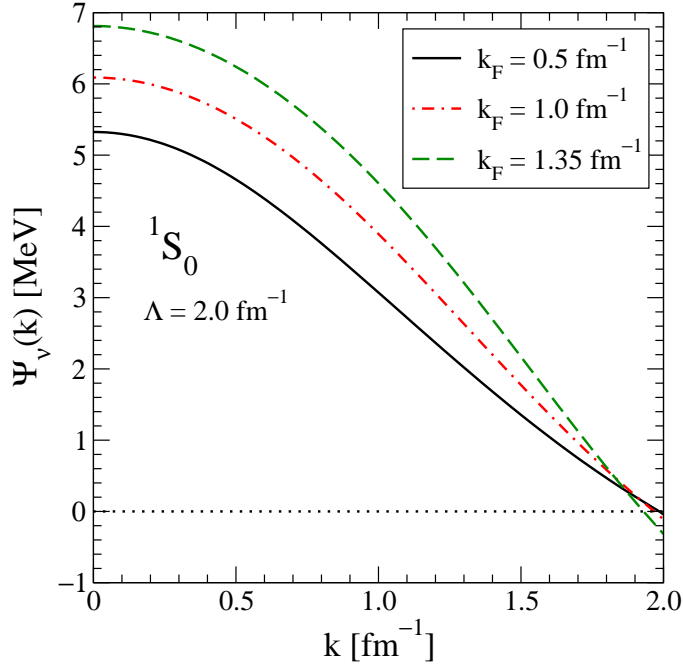


Fig. 8. Momentum dependence of the eigenvector corresponding to the largest attractive eigenvalue at  $\omega = 0$  for representative  $k_F$  values. This serves as the first approximation to the gap function.

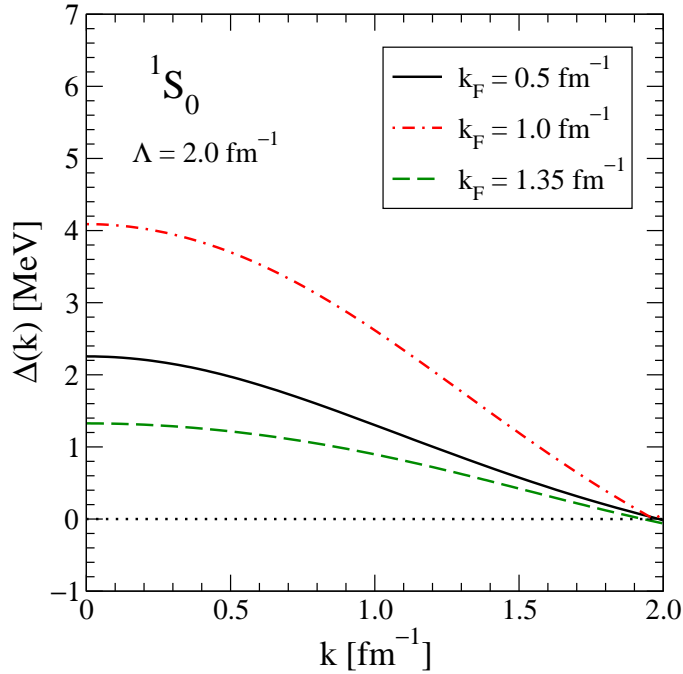


Fig. 9. Momentum dependence of the self-consistent gap function  $\Delta(k)$ , obtained from the Weinberg eigenvectors corresponding to the largest attractive eigenvalue at  $\omega = 0$  as the initial gap function.

Apart from some small numerical instabilities outside the  $\pm 2\Delta_F$  region, the largest eigenvalue behaves like the eigenvalue in the separable case as  $E \rightarrow 2\mu$  (see Fig. 6). Similarly, the eigenvector corresponding to  $\eta_\nu^{\text{NG}}(E) = 1$  as  $E \rightarrow 2\mu$  is an approximation to the gap function. Figure 8 shows the eigenvector corresponding to the largest eigenvalue at  $E = 2\mu$  for representative densities. Using this as the first guess for the gap function  $\Delta(k)$  and iterating the gap equation,

$$\Delta(k) = -\frac{1}{\pi} \int_0^\infty q^2 dq \frac{V(k, q)\Delta(q)}{\sqrt{\xi_q^2 + \Delta(q)^2}}, \quad (32)$$

yields the self-consistent BCS gap function, which is shown in Fig. 9. It is evident that the non-self-consistent eigenvector is a poor approximation to  $\Delta(k)$  in general. As  $k_F$  increases, the gap closes for smaller momentum values, as observed in Ref. [19]. These results are consistent with the density dependence of the  $^1S_0$  gap  $\Delta_F$ .

## 4 Summary

In summary, we see that pairing instability is reflected in the behavior of the Weinberg eigenvalues close to the Fermi surface, with the signature of non-perturbativeness given by the presence of eigenvalues outside the unit circle. We find that a good approximation to the momentum independent gaps  $\Delta_F$  can be obtained from a stability analysis, which means that weak coupling is a good approximation for low-momentum interactions. If instead we use the Nambu-Gorkov two-particle Green's function, the largest attractive eigenvalue tends to one close to the Fermi surface, indicating the presence of bound states (Cooper pairs). At the Fermi surface, the eigenvalue equation is the gap equation and the self-consistent eigenvector corresponding to the largest attractive eigenvalue is the gap function.

The gaps we have shown correspond to the BCS results and do not include polarization effects. These effects are known to significantly reduce the gap in neutron matter [16,20,15,21,22]. These interactions can be taken into account within this framework using the potential

$$V(k', k) = V_0(k', k) + V_{\text{ind}}(k', k), \quad (33)$$

where  $V_0(k', k)$  is the two-body interaction and  $V_{\text{ind}}(k', k)$  is the induced interaction, given in detail in Refs. [20,23]. Once again we use the two-particle Green's function,  $G_{pphh}^0$ , to calculate the eigenvalues close to the Fermi-surface and determine the pairing gap at  $k_F$  in a similar fashion. This method therefore offers an extension to include medium effects.

Any residual cutoff dependence in the gaps suggests the importance of many-

body forces. Our results agree with the recent work of Hebeler et al [12] that shows that the cutoff dependence of the  $^1S_0$  gap in neutron matter is weak. As a result the three-nucleon contribution to the  $^1S_0$  pairing gaps in neutron matter is expected to be small at the BCS level. A preliminary analysis for the  $^3S_1$  gaps in nuclear matter exhibit strong cutoff dependences and hence it would be worthwhile to investigate the role of three-nucleon interactions and the corresponding medium effects.

The success of the in-medium Weinberg analysis for pairing suggests that it should be useful in assessing other possible sources of nonperturbative physics. Recent results by Roth and collaborators [24] indicate that, for low-momentum potentials, correlation effects in finite nuclei beyond second order do not significantly change the binding energy per nucleon. This motivates us to investigate the perturbativeness of the particle-hole channel for bulk nuclear matter using the Weinberg eigenvalue analysis, which is in progress.

## Acknowledgements

We thank Achim Schwenk for useful comments and discussions. This work was supported in part by the National Science Foundation under Grant Nos. PHY-0354916 and PHY-0653312 and by the U.S. Department of Energy under grant DE-FG02-93ER40756.

## References

- [1] S. Weinberg, *Phys. Rev.* **131** (1963) 440.
- [2] W. Glöckle, *The Quantum Mechanical Few-Body Problem* (Springer-Verlag, Berlin, 1983).
- [3] S. K. Bogner, R. J. Furnstahl, S. Ramanan and A. Schwenk, *Nucl. Phys.* **A773** (2006) 203.
- [4] S. K. Bogner, R. J. Furnstahl, S. Ramanan and A. Schwenk, *Nucl. Phys.* **A784** (2007) 79.
- [5] S. K. Bogner, R. J. Furnstahl and R. J. Perry, *Phys. Rev. C* **75** (2007) 061001.
- [6] R. B. Wiringa, V. G. J. Stoks and R. Schiavilla, *Phys. Rev. C* **51** (1995) 38.
- [7] D. R. Entem and R. Machleidt, *Phys. Rev. C* **68** (2003) 041001(R);  
E. Epelbaum, W. Glöckle, Ulf-G. Meißner, *Nucl. Phys.* **A747** (2005) 362.
- [8] S.K. Bogner, A. Schwenk, T.T.S. Kuo and G.E. Brown, nucl-th/0111042.

- [9] S. K. Bogner, T. T. S. Kuo, A. Schwenk, D. R. Entem and R. Machleidt, Phys. Lett. B **576** (2003) 265;  
S. K. Bogner, T. T. S. Kuo and A. Schwenk, Phys. Rept. **386** (2003) 1.
- [10] S. K. Bogner, A. Schwenk, R. J. Furnstahl and A. Nogga, Nucl. Phys. **A763** (2005) 59.
- [11] S. K. Bogner and R. J. Furnstahl, Phys. Lett. B **632** (2006) 501.
- [12] K. Hebeler, A. Schwenk, B. Friman, Phys. Lett. B **648** (2007) 176.
- [13] J. R. Schrieffer, *Theory of Superconductivity* (Perseus Books, New York, 1999).
- [14] A. L. Fetter and J. D. Walecka, *Quantum Theory of Many-Particle Systems* (Dover Publications, New York, 2002).
- [15] U. Lombardo and H. J. Schulze, Lect. Notes Phys. **578** (2001) 30.
- [16] A. Schwenk, B. Friman and G. E. Brown, Nucl. Phys. **A713** (2003) 191.
- [17] W. H. Dickhoff and D. Van Neck, *Many-Body Theory Exposed!* (World Scientific, Singapore 2005).
- [18] A. A. Abrikosov, L. P. Gorkov and I. E. Dzyaloshinski, *Methods of Quantum Field Theory in Statistical Physics* (Dover Publications, New York, 1975).
- [19] V. A. Khodel, V. V. Khodel and J. W. Clark, Nucl. Phys. **A598** (1996) 390.
- [20] H. Heiselberg, C. J. Pethick, H. Smith, and L. Viverit, Phys. Rev. Lett. **85** (2000) 2418.
- [21] A. Schwenk, Int. J. Mod. Phys. **B20** (2006) 2724.
- [22] A. Schwenk, AIP Conf. Proc. **892** (2007) 502 [arXiv:nucl-th/0611046].
- [23] H. -J. Schulze, J. Cugnon, A. Lejeune, M. Baldo and U. Lombardo, Phys. Lett. B **375** (1996) 1.
- [24] R. Roth, P. Papakonstantinou, N. Paar, H. Hergert, T. Neff and H. Feldmeier, Phys. Rev. C **73** (2006) 044312;  
C. Barbieri, N. Paar, R. Roth, and P. Papakonstantinou, arXiv:nucl-th/0608011.